nature chemistry

SUPPLEMENTARY INFORMATION

DOI: 10.1038/NCHEM.2447

Chemical amplification of magnetic field effects relevant to avian magnetoreception

Daniel R. Kattnig, Emrys W. Evans, Victoire Déjean, Charlotte A. Dodson, Mark I. Wallace, Stuart R. Mackenzie, Christiane R. Timmel, P. J. Hore

Contents

A. Measurement of magnetic field effects by fluorescence

Spectrally resolved MFEs: Setup I

Magnetic field effects on fluorescence spectra were recorded essentially as described by Evans *et al*.[1] Samples were positioned between Helmholtz coils which were used to generate static magnetic fields of up to 12 mT, with rise and fall times less than 3 ms. A 405 nm CW diode laser (1Q1H350, 350 mW; Power Technology) provided continuous illumination of the sample. The fluorescence was coupled to a spectrograph (SR303i; Andor) which dispersed the wavelength components onto a charge-coupled device (CCD) camera (DU90P-BV; Andor Newton). The fluorescence signal was integrated for a defined period (the camera 'exposure time') starting at a fixed 'delay time', *T*, after switching on the magnetic field. After recording the signal, the field was returned to zero ready for the next measurement. Most solutions were flowed at a rate of *ca*. 0.25 mL min^{-1} through a sample cell (Starna Scientific, UV Quartz, 45/Q, 1 mm optical path length) so as to minimize photodegradation. Most of the experiments were conducted at room temperature and for magnetic fields in the range 0 to 12 mT, chosen in a randomized order. For *At*Cry1, the sample was not flowed and was cooled (282 K) using a custom-made, chilled stage.

Experimental parameters for the results presented in the main text are given in Supplementary Table A1.

Figure	Sample	delay time	exposure time	excitation power	averages
2c	FMN/lysozyme	10, 50 ms	20 ms	270 mW	300
		0.5 s	20 ms	270 mW	100
		2.0 s	20 ms	270 mW	75
		5.0 s	20 ms	270 mW	35
4a	FMN/ascorbic acid	50 ms	20 ms	350 mW	900
6a	*At*Cry1	0.5, 1.0 s	0.5 s	1 mW	300
		3.5 s	0.5 s	1 mW	80

Supplementary Table A1. Setup I: Experimental parameters for the measurements shown in the main text.

Time-resolved MFEs: Setup II

Time-resolved measurements were carried out using an inverted fluorescence microscope (Ti-E; Nikon). Samples were held in a flow chamber constructed from a silicon rubber gasket (McMaster-Carr) and two coverslips (Menzel; Germany) with an optical path length of 0.5 mm (see Ref.[2]). They were illuminated using the attenuated and expanded beam of a 470 nm diode laser (Stradus 473-80, 80 mW; Vortran Laser Technology). The excitation light was focused at the back aperture of an oil immersion objective (CFI Apo TIRF 60X Oil, N.A. 1.49; Nikon) to provide trans-illumination of the sample. The power entering the back of the objective was varied between 0.10 and 3.7 mW resulting in power densities in the object plane between 0.020 and 0.74 μW $μm^{-2}$ (based on the $1/e^2$ contours of the excitation intensity). The fluorescence emission was collected through the same objective,

transmitted through a dichroic mirror (Brightline FF497-Di03; Semrock) and a bandpass filter (BrightLine 550/88; Semrock), and recorded using an electron-multiplying CCD camera (iXon+ DV860E; Andor Technology). Magnetic fields were generated using a solenoid wound around a 3 mm diameter ferrite core and fixed into a non-metallic mount placed 1 mm above the sample. Using a custom-built power supply, magnetic fields of up to 27 mT could be generated with a rise time of less than 70 µs. Both the data acquisition and the magnetic field stepping were controlled by a digital delay pulse generator (model 9520; Quantum Composers). The excitation light was only admitted to the sample during the fluorescence measurement period using an optical shutter (SH05; Thorlabs) synchronized with the camera shutter. A description of the calibration of the magnetic field can be found in Ref.[3].

Experimental parameters for the results presented in the main text are given in Supplementary Table A2.

For all samples except cryptochrome (Fig. 6, main text), the fluorescence was integrated for a period of 5 ms per camera frame (the camera 'exposure time') and the interval between frames was 7 ms (frame rate: ~143 Hz). Typically 16,000 frames were recorded with the magnetic field alternated between zero and a preset value every 80, 160, or 240 frames depending on the sample (see Supplementary Table A2 for details of individual measurements). The 'field on/off interval' is the time the magnetic field remains on or off before switching. For each run, a previously unexposed aliquot of the sample was admitted to the cell using a flow system. The flow was stopped while the fluorescence was measured.

For the cryptochrome experiments, 50 µL samples were held between two coverslips separated by a polydimethylsiloxane spacer (Sylgard 184; Dow Corning). The sample was injected into the pre-cooled cell placed on a Peltier stage (PT100-NIF; Linkam) at 268 K. 10,000 frames were recorded with an exposure time of 40 ms and frame interval of 42 ms with the field switched every 100 frames (i.e. 4.2 s). For each measurement at least 11 time-traces were accumulated, each time using a previously unexposed portion of the sample.

Figure	Sample	frame interval	exposure time	frames	field on/off interval	excitation power	traces
2a,b	FMN/lysozyme	7 ms	5 ms	16,000	1.68 s	0.24 mW	16
2d,e	FMN/tryptophan	7 ms	5 ms	16,000	0.56 s	3.7 mW	25
2f	FMN/ tryptophan (+TCEP or at pH = 2.6)	7 ms	5 ms	16,000	1.12 s	3.7 mW	6,7
4b,c	FMN/ascorbic acid	7 ms	5 ms	16,000	1.12 s	3.7 mW	35,63
6b,c	*At*Cry1	42 ms	40 ms	10,000	4.2 s	0.1 mW	15,11

Supplementary Table A2. Setup II: Experimental parameters for the measurements shown in the main text.

The fluorescence intensity for each camera frame was obtained by 'robust averaging'.[4] To determine the time-resolved MFE, the fluorescence time-profiles from individual measurements (as described above) were averaged, fitted to a multi-exponential function and used to calculate the MFEs for each field-on/field-off cycle. The first 5 cycles were discarded because of distortions resulting from

the system adjusting to a new quasi-equilibrium during the initial phase of photoexcitation and because there was some difficulty fitting the average intensity due to the steep decay of the fluorescence at the beginning of the measurement. The time-resolved MFEs for the remaining on/off-cycles were averaged with the smallest and largest 5% of the values at every time point removed in order to guard against outliers and spikes. There were no statistically significant differences (at the 95% level) between the remaining time points and their means. In order to determine the prompt and the delayed MFEs, the time-resolved MFEs were fitted to exponential functions starting with the fourth time point. The MFEs extrapolated to $t = 0$ and $t \rightarrow \infty$ are reported as χ_p and χ_d, respectively.

B. Measurement of magnetic field effects on intermolecular reactions of flavins

FMN/Lysozyme

Using setup I, fluorescence-detected MFE profiles were recorded for FMN/lysozyme mixtures at various delay times, T, between switching on the magnetic field and recording the fluorescence. A 10 µM FMN/0.5 mM lysozyme sample was flowed at 0.25 mL min^{-1} with continuous photoexcitation by a 405 nm laser at 270 mW. The fluorescence spectral profile showed good agreement with the $S_1 \rightarrow S_0$, $\pi\pi^*$ transition of the isoalloxazine group of the flavin. A small decrease in fluorescence intensity was seen on application of an external magnetic field (12 mT). The inverted, scaled fluorescence difference signal for T = 0.01 s, $\Delta I_F(B_0) = I_F(B_0) - I_F(0)$, is shown as the black trace in Supplementary Fig. B1a; its sign is consistent with an initial *triplet* radical pair. The difference spectrum coincides perfectly with the fluorescence profile of fully oxidised FMN (red trace), suggesting a single dominant, magnetically sensitive fluorescent species (the excited singlet state of fully oxidised FMN). This conclusion is reinforced by the coincidence of the scaled difference signals obtained for different delay times between the field change and the start of fluorescence acquisition (Supplementary Fig. B1b).

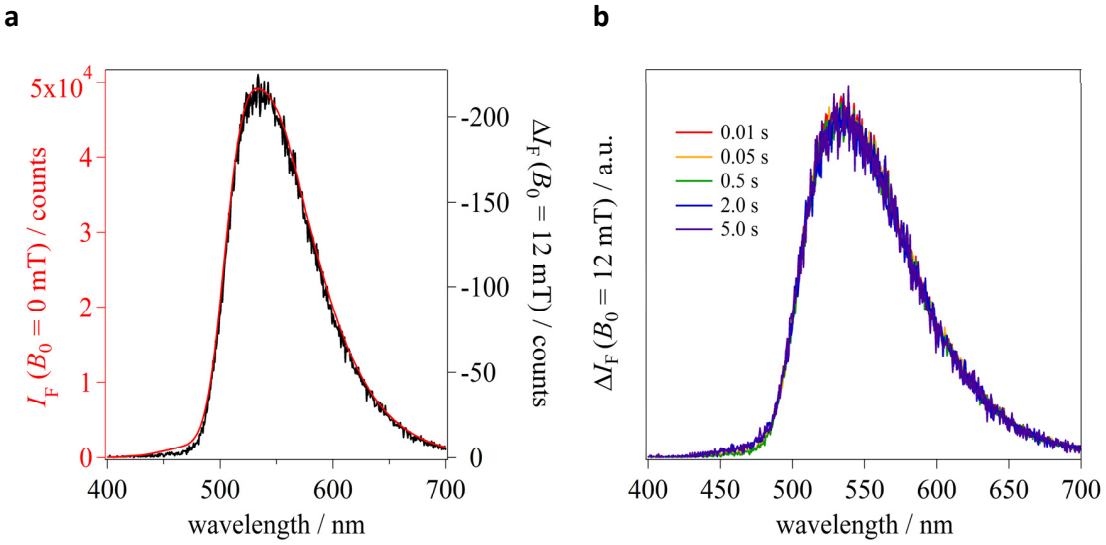

Supplementary Figure B1. a, Superimposed fluorescence intensity $I_F(B_0 = 0)$ (red) and difference spectra $\Delta I_F(B_0 = 12\ mT)$ (black) for 10 µM FMN + 0.5 mM lysozyme in water. Delay time, T = 0.01 s. **b**, Scaled difference spectra for the same system at different delay times between the field step and the start of fluorescence acquisition.

In Fig. 2c of the main text, an MFE amplification (averaged over 500-600 nm) was observed with increasing delay time T, whilst the $B_{1/2}$ (magnetic field strength corresponding to half of the maximum MFE) is unchanged (Supplementary Table B1). The invariance of $B_{1/2}$ is in keeping with our proposal that the enhanced MFEs stem from a single radical pair.

delay / s	0.01	0.05	0.5	2.0	5.0
$B_{1/2}$ / mT	6.3 ± 0.1	6.5 ± 0.2	6.5 ± 0.3	6.5 ± 0.2	6.3 ± 0.3

Supplementary Table B1. Values of $B_{1/2}$ determined from the data shown in Fig. 2c.

Setup II was used to investigate the time-dependence of the enhanced MFE. Fresh samples were continuously illuminated in the presence of a magnetic field stepped between 0 mT and 27 mT (rise time < 70 μs) recording the fluorescence continuously. The overall decrease in fluorescence intensity (Fig. 2a and d, main text) is due to the sample re-equilibrating to photoexcitation and the interplay between photobleaching and diffusion. Turning on the photoexcitation source rapidly depletes the flavin ground state as steady state concentrations for the excited states are reached. The photochemistry of flavins is not as perfectly cyclic as implied by the reaction scheme in Fig. 1 (main text). Photoexcitation also leads to degradation products such as lumichrome.[5] Although lumichrome is also capable of forming photo-induced triplet-born radical pairs, no magnetically sensitive fluorescence from lumichrome was observable with 470 nm photoexcitation in setup II. Such photodegradation pathways tend to reduce the measured fluorescence intensity, although this is opposed by diffusion of fresh sample into the detection volume.

As mentioned in the main text, the time-resolved MFE is superimposed on the decaying trend of the fluorescence. An average MFE response to field switching was obtained following the subtraction of the decay by means of multi-exponential fits. No statistically significant difference was observed when comparing individual cycles to their means. Furthermore, the averaged MFE responses to field-on and field-off steps were identical (see Supplementary Fig. B2).

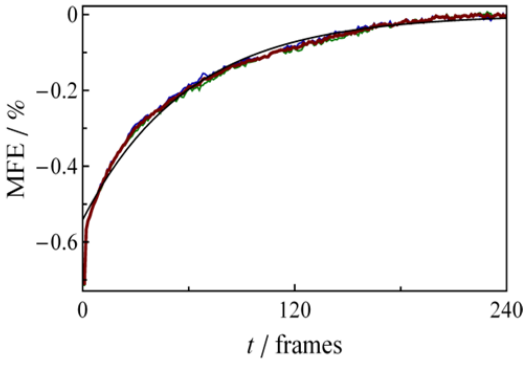

Supplementary Figure B2. Averaged MFEs for field-on and field-off steps. Green: response to switching field on. Blue: response to switching field off. Red: average of the two. Black: exponential fit.

To obtain the enhancement factor, E, the initial (primary, χ_p) and final (delayed, χ_d) MFEs were determined. An exponential function was fitted to the slow component (see, e.g., Supplementary Fig. B2) to obtain a time constant (τ). Using such fits values of χ_d could be obtained for reactions that did not reach a steady state during the field on/off periods.

Increasing the solvent viscosity of the FMN/lysozyme solutions by the addition of glycerol (20% v/v) was found to boost the enhancement (Supplementary Fig. B3) from 2.32 to 3.50, as well as increasing the time constant from τ = 0.47 s to τ = 2.2 s. While the ratio of the two termination rate constants (k_D/k_F) determines E, it is their values which set the timescale. It seems likely that the increase in solvent viscosity affects the diffusion-controlled contributions to k_D and k_F and hence both E and τ.

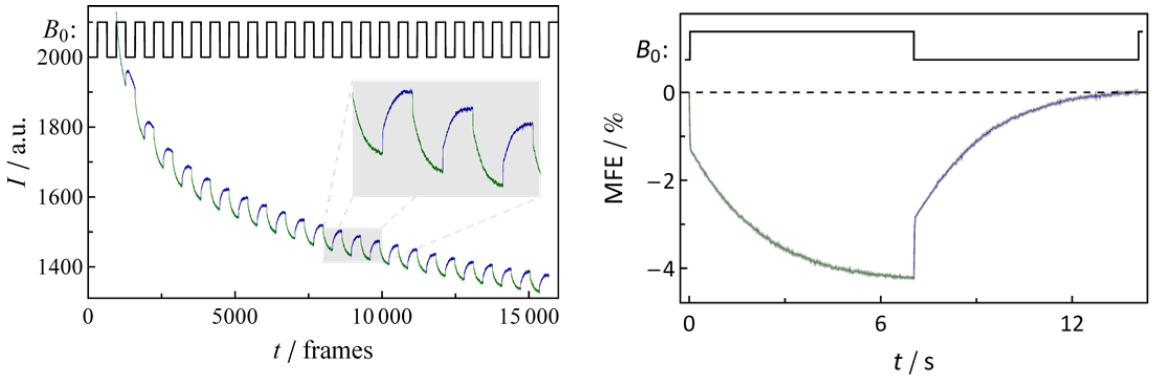

Supplementary Figure B3. Left: Fluorescence intensity profile for 10 µM FMN + 0.5 mM lysozyme (20% v/v glycerol in water) in the presence of a square wave modulated magnetic field (0 to 27 mT) using Setup II. **Right**: the averaged response to a single field step.

FMN/Tryptophan

The rate of disappearance of flavin radicals by disproportionation and reaction with molecular oxygen increases supra-linearly with their concentration as a result of the quadratic and autocatalytic nature, respectively, of the two processes. As expected and shown in Supplementary Figs B4 and B5, increasing either the FMN concentration or the laser pump power increases k_F, decreases k_D/k_F and results in smaller enhancement factors.

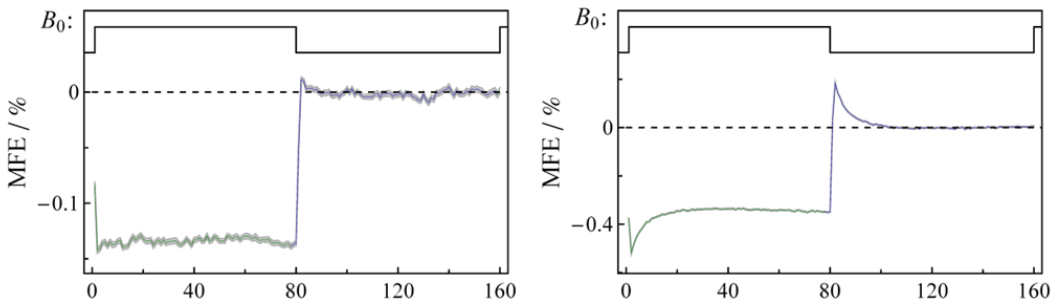

Supplementary Figure B4. Averaged MFE responses to a single field step (0–27 mT) for 10 µM FMN + 1.0 mM tryptophan with varying laser pump power (470 nm): **left**, 0.24 mW and **right**, 3.7 mW.

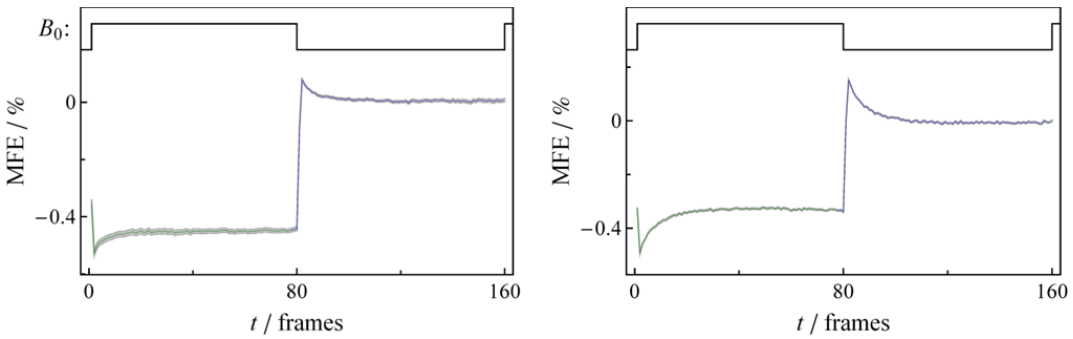

Supplementary Figure B5. Averaged MFE responses to a single field step (0–27 mT) for FMN + 1.0 mM tryptophan for different flavin concentrations: **left**, 2.5 µM and **right**, 10 µM.

C. Calculation of MFEs for inter- and intramolecular radical pairs

Intermolecular MFEs

The reaction scheme in Supplementary Fig. C1 has been used to model the MFEs that arise in cyclic intermolecular radical pair reactions under conditions of continuous illumination and square-wave modulated magnetic fields. Using an approach analogous to that of Murakami *et al*.[6], we have solved numerically the differential equations that describe the time-dependence of the system following step-wise changes in the intensity of an external magnetic field.

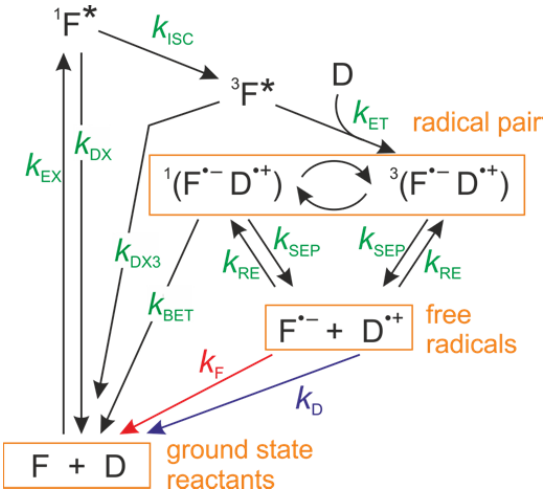

Supplementary Figure C1. Reaction scheme for intermolecular flavin (F) + donor (D) reactions.

The magnetic sensitivity of the photocycle originates in field-dependent singlet-triplet interconversion of the singlet (S) and triplet (T_0, T_+, T_-) spin states of the geminate radical pair (curly arrows in Supplementary Fig. C1). The field-independent rate equations for species other than the radical pair are:

$$\begin{aligned}
\frac{\mathrm{d}}{\mathrm{d}t}[\mathrm{F}] &= -k_{\mathrm{EX}}[\mathrm{F}] + k_{\mathrm{DX}}[^1\mathrm{F}^*] + k_{\mathrm{DX3}}[^3\mathrm{F}^*] + k_{\mathrm{BET}}[\mathrm{S}_0] + k_{\mathrm{F}}[\mathrm{F}^{\bullet-}] \\
\frac{\mathrm{d}}{\mathrm{d}t}[^1\mathrm{F}^*] &= -\left(k_{\mathrm{ISC}} + k_{\mathrm{DX}}\right)[^1\mathrm{F}^*] + k_{\mathrm{EX}}[\mathrm{F}] \\
\frac{\mathrm{d}}{\mathrm{d}t}[^3\mathrm{F}^*] &= -\left(k_{\mathrm{ET}}[\mathrm{D}] + k_{\mathrm{DX3}}\right)[^3\mathrm{F}^*] + k_{\mathrm{ISC}}[^1\mathrm{F}^*] \\
\frac{\mathrm{d}}{\mathrm{d}t}[\mathrm{F}^{\bullet-}] &= -\left(k_{\mathrm{RE}}[\mathrm{D}^{\bullet+}] + k_{\mathrm{F}}\right)[\mathrm{F}^{\bullet-}] + k_{\mathrm{SEP}}\left([\mathrm{S}] + [\mathrm{T}_0] + [\mathrm{T}_+] + [\mathrm{T}_-]\right) \\
\frac{\mathrm{d}}{\mathrm{d}t}[\mathrm{D}] &= -k_{\mathrm{ET}}[^3\mathrm{F}^*][\mathrm{D}] + k_{\mathrm{BET}}[\mathrm{S}] + k_{\mathrm{D}}[\mathrm{D}^{\bullet+}] \\
\frac{\mathrm{d}}{\mathrm{d}t}[\mathrm{D}^{\bullet+}] &= -\left(k_{\mathrm{RE}}[\mathrm{F}^{\bullet-}] + k_{\mathrm{D}}\right)[\mathrm{D}^{\bullet+}] + k_{\mathrm{SEP}}\left([\mathrm{S}] + [\mathrm{T}_0] + [\mathrm{T}_+] + [\mathrm{T}_-]\right).
\end{aligned} \tag{1}$$

Note that the first terms on the right hand side of the 4th and 6th equations (rate constant k_{RE}) do not change the total flavin or donor radical concentrations, merely whether these species are

present in the radical pair or as free radicals. The concentrations of the latter greatly exceed those of the former.

In the absence of a magnetic field, all four spin states of the radical pair can interconvert with each other via the hyperfine interactions with the rate constant k_{HFM}:

$$\begin{aligned}
\frac{d}{dt}[S] &= -(3k_{HFM} + k_{BET} + k_{SEP})[S] + k_{HFM}([T_0] + [T_+] + [T_-]) + \frac{1}{4}k_{RE}[F^{\bullet -}][D^{\bullet +}] \\
\frac{d}{dt}[T_0] &= -(3k_{HFM} + k_{SEP})[T_0] + k_{HFM}([S] + [T_+] + [T_-]) + \frac{1}{4}k_{RE}[F^{\bullet -}][D^{\bullet +}] + \frac{1}{3}k_{ET}[^3F^*][D] \\
\frac{d}{dt}[T_+] &= -(2k_{HFM} + k_{SEP})[T_+] + k_{HFM}([S] + [T_0]) + \frac{1}{4}k_{RE}[F^{\bullet -}][D^{\bullet +}] + \frac{1}{3}k_{ET}[^3F^*][D] \\
\frac{d}{dt}[T_-] &= -(2k_{HFM} + k_{SEP})[T_-] + k_{HFM}([S] + [T_0]) + \frac{1}{4}k_{RE}[F^{\bullet -}][D^{\bullet +}] + \frac{1}{3}k_{ET}[^3F^*][D].
\end{aligned} \tag{2}$$

At high magnetic field, the T_+ and T_- states become energetically separated from S and T_0 by the Zeeman interaction. This disables $ST_\pm$ interconversion such that the rate equations for the geminate radical pair become:

$$\begin{aligned}
\frac{d}{dt}[S] &= -(k_{HFM} + 2k_{RM} + k_{BET} + k_{SEP})[S] + k_{HFM}[T_0] + k_{RM}([T_+] + [T_-]) + \frac{1}{4}k_{RE}[F^{\bullet -}][D^{\bullet +}] \\
\frac{d}{dt}[T_0] &= -(k_{HFM} + 2k_{RM} + k_{SEP})[T_0] + k_{HFM}[S] + k_{RM}([T_+] + [T_-]) + \frac{1}{4}k_{RE}[F^{\bullet -}][D^{\bullet +}] + \frac{1}{3}k_{ET}[^3F^*][D] \\
\frac{d}{dt}[T_+] &= -(2k_{RM} + k_{SEP})[T_+] + k_{RM}([S] + [T_0]) + \frac{1}{4}k_{RE}[F^{\bullet -}][D^{\bullet +}] + \frac{1}{3}k_{ET}[^3F^*][D] \\
\frac{d}{dt}[T_-] &= -(2k_{RM} + k_{SEP})[T_-] + k_{RM}([S] + [T_0]) + \frac{1}{4}k_{RE}[F^{\bullet -}][D^{\bullet +}] + \frac{1}{3}k_{ET}[^3F^*][D]
\end{aligned} \tag{3}$$

k_{RM} is the rate constant for incoherent spin mixing resulting from spin relaxation processes. Supplementary Fig. C2 indicates the pathways described by the rate constants k_{HFM} and k_{RM}.

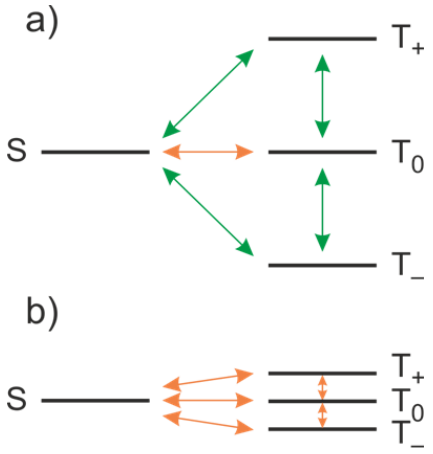

Supplementary Figure C2. Hyperfine mixing (orange arrows, rate constant k_{HFM}) and spin relaxation (green arrows, rate constant k_{RM}) at **a** high field and **b** low field.

MATLAB's 15s ordinary differential equation solver was used to calculate the change in the concentration of ground state flavin when the applied magnetic field was switched on and off under conditions of continuous photoexcitation. The fluorescence intensity is directly proportional to [F].

Calculations were performed using the rate constants in Supplementary Table C1. As shown in Fig. 3a (main text), this yielded: (i) step-wise behaviour (enhancement factor, $E = \chi_e/\chi_d = 1$) in the absence of termination channels ($k_F = k_D = 0$); (ii) $E > 1$ for $k_D/k_F > 1$; (iii) $E < 1$ for $k_D/k_F < 1$. Similar calculations were used to obtain the contour plot in Fig. 3b (main text) showing the dependence of E on k_D / k_F for k_D and k_F in the range 10^{-1}–10^3 s^{-1}. The simulations used to obtain values of k_D and k_F from the data in Figs 2b, e and f, 4b and c, and 6b and c were barely affected by the rates of the other reaction steps (Supplementary Table C1) which, for the small values of k_D and k_F relevant here, determine solely the prompt MFE.

In determining E, the final MFE response (χ_d) was obtained from the steady state solution to Equations (1)–(3). The initial MFE (χ_p) was defined at the moment of instantaneous magnetic field switching and was determined from the exponential fit to the enhanced MFE.

Rate constant	*Value*	*Comment*
k_{EX}	1.36×10^4 s^{-1}	Photoexcitation is assumed to follow first order kinetics in the weak absorbance limit of the Beer-Lambert law.
k_{DX}	1.09×10^8 s^{-1}	Decay of the flavin excited singlet state (^{1}F*) by processes other than intersystem-crossing.[7, 8]
k_{ISC}	1.09×10^8 s^{-1}	Intersystem crossing from ^{1}F* to ^{3}F*[7, 8].
k_{ET}	1.2×10^9 $M^{-1}s^{-1}$	Reaction of the flavin excited triplet state (^{3}F*) with an electron donor, D. The numerical value was derived from Stern-Volmer type experiments on flavin mononucleotide (FMN) + tryptophan reactions using transient absorption spectroscopy (see Section C).
k_{DX3}	3.85×10^5 s^{-1}	Decay of ^{3}F* by processes other than quenching by D. The numerical value was taken from transient absorption experiments on FMN (see Section C).
k_{SEP}	2×10^8 s^{-1}	Separation of geminate radical pair components to form free radicals. The value is based on a typical geminate radical pair lifetime of 100 ns in aqueous solution.
k_{HFM}	8×10^7 s^{-1}	Coherent singlet-triplet interconversion of the spin states of the geminate radical pair by the hyperfine mechanism as determined by Murakami *et al*.[6]
k_{RM}	2×10^6 s^{-1}	Incoherent singlet-triplet interconversion of the spin states of the geminate radical pair by the relaxation mechanism as determined by Murakami *et al*.[6]
k_{RE}	1.87×10^{10} M^{-1} s^{-1}	Re-encounter of free radicals to form geminate radical pair. The value is obtained from the Smoluchowski equation (with an effective encounter distance, R^* = 20 Å) and the Stokes-Einstein relation (T = 295 K; species radius, R = 3.5 Å; solvent viscosity = 1×10^{-2} kg m^{-1} s^{-1}).

k_{BET}	1.0×10^8 s^{-1}	Spin-selective reverse electron transfer of the radical pair to form the ground state reactants.

Supplementary Table C1. Values of the rate constants used in calculations of amplified MFEs for the intermolecular flavin photocycle in Supplementary Fig. C1.

Lower light intensities lead to larger enhancements

Fig. 3b (main text) shows the dependence of E on k_D and k_F for a typical intermolecular flavin-containing radical pair. Those calculations used the values of the rate constants given in Supplementary Table C1; the resultant density plot is also given below (Supplementary Fig. C3a) together with plots of the constituent delayed (χ_d) and prompt (χ_p) MFEs (Supplementary Figs. C3b and C3c, respectively).

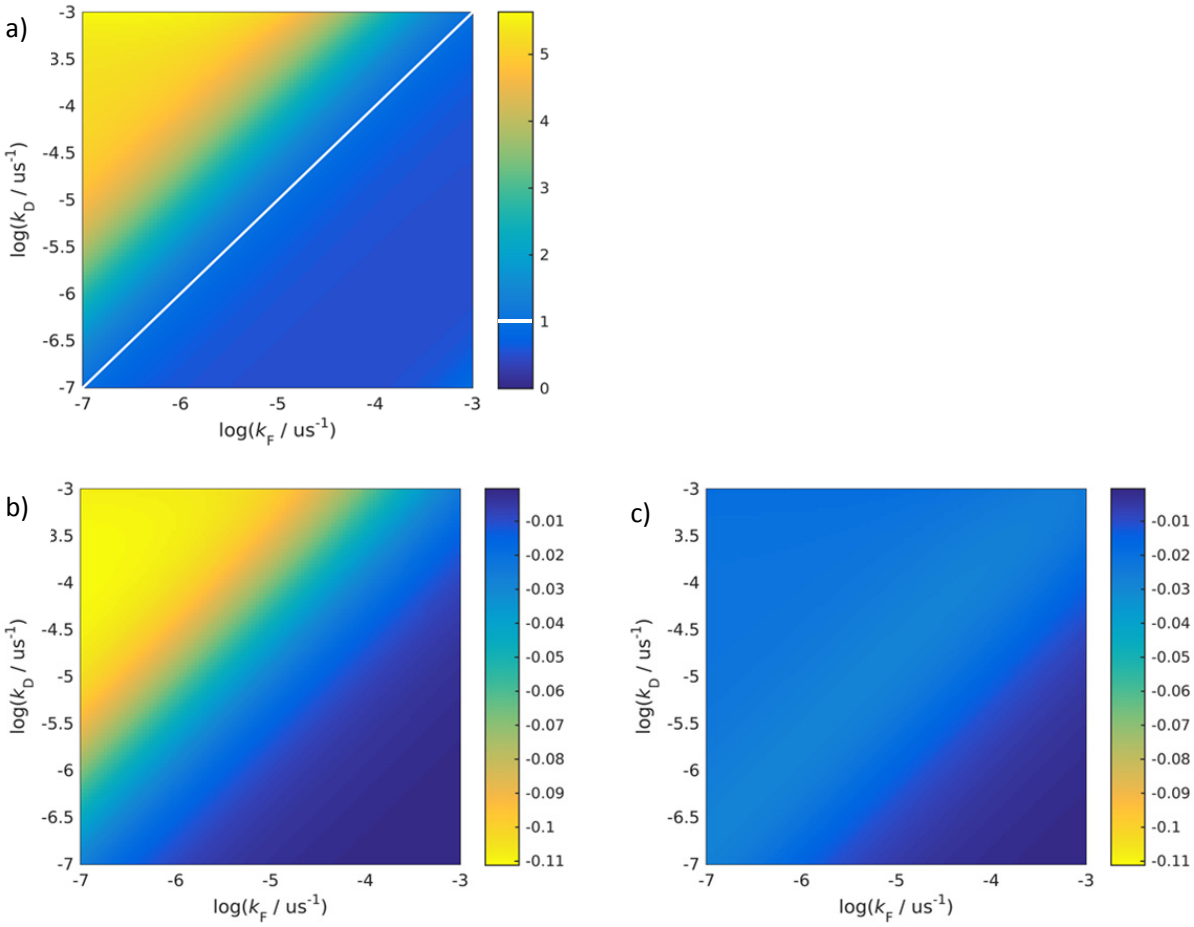

Supplementary Figure C3. Intermolecular radical pair. Density plots of: **a**, the amplification factor, E; **b**, the delayed MFE, χ_d; **c** the prompt MFE, χ_p, as a function of the radical termination rate constants k_F and k_D. The simulations were performed using the rate constant values in Supplementary Table C1 with $k_{EX} = 1.36 \times 10^4$ s^{-1}.

As mentioned in the main text, larger MFE amplifications can be realized with lower light intensities. The calculated behaviour for a sample subjected to 20% of the photon flux (i.e. $k_{EX} = 2.72 \times 10^3\ s^{-1}$) is shown in Supplementary Fig. C4. Enhancement factors of up to 24 are observed in the range of k_F and k_D values covered.

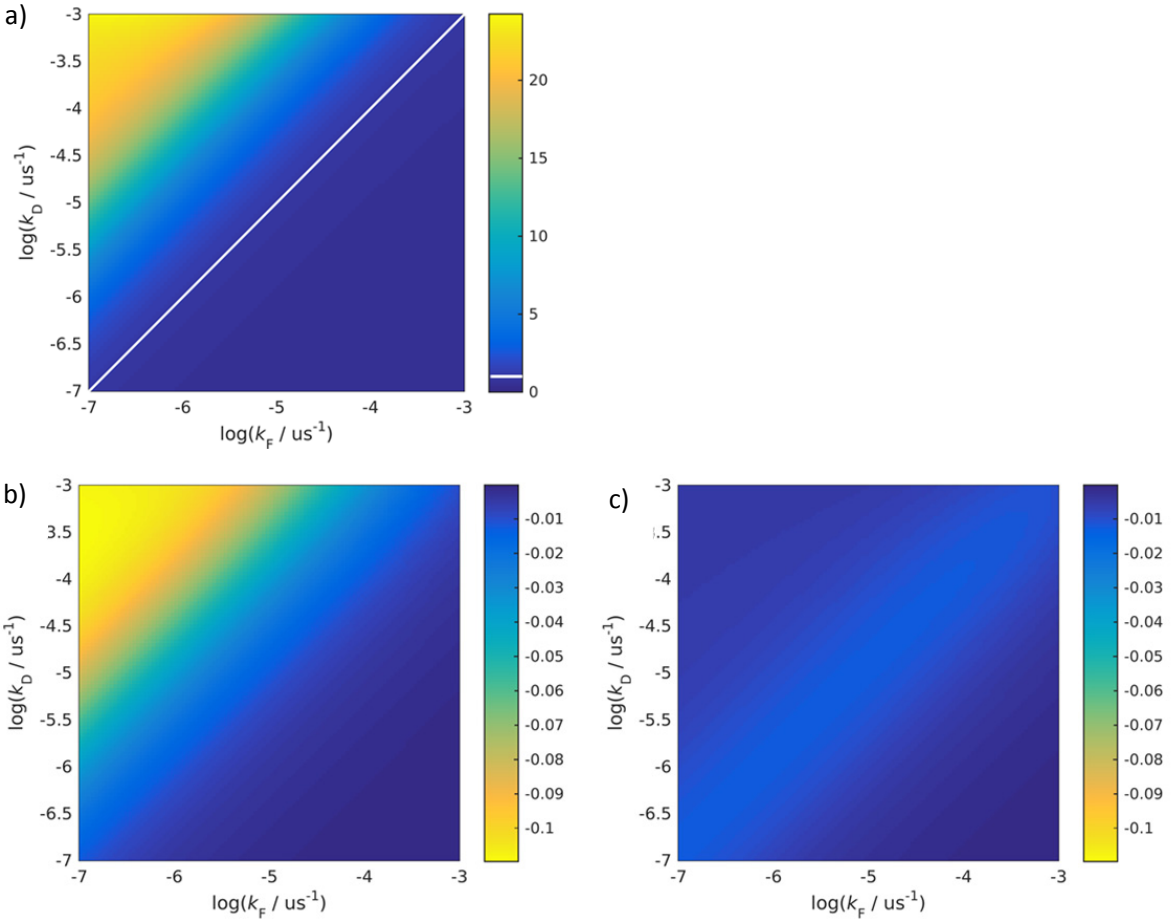

Supplementary Figure C4. Intermolecular radical pair. Density plots of: **a**, the amplification factor, *E*; **b**, the delayed MFE, χ_d; **c**, the prompt MFE, χ_p, as a function of the radical termination rate constants k_F and k_D. The simulations were performed using the rate constant values in Supplementary Table C1 except for $k_{EX} = 2.72 \times 10^3\ s^{-1}$.

Intramolecular MFEs

Analogous calculations of EMFEs were conducted for an intramolecular photocycle based on cryptochrome (Supplementary Fig. C5 and Supplementary Table C2). The corresponding density plots are shown in Supplementary Fig. C6-C8.

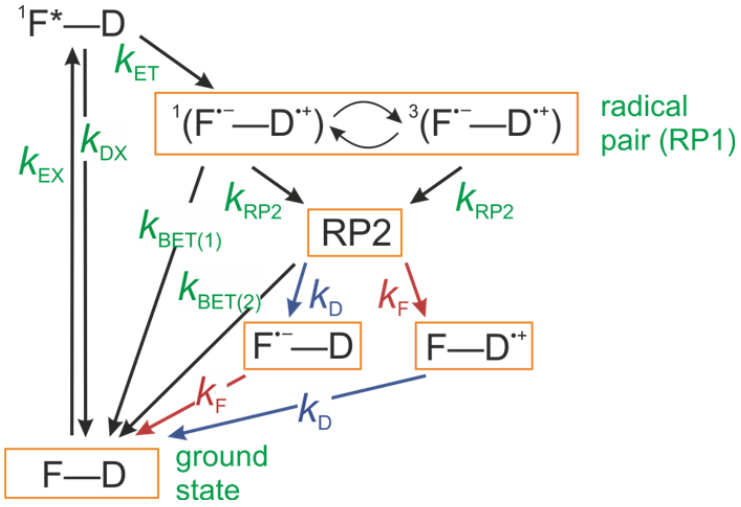

Supplementary Figure C5. Reaction scheme for an intramolecular radical pair reaction modelled on a typical cryptochrome photocycle.

Rate constant	*Value*	*Comment*
k_{EX}	1×10^3 s^{-1}	Photoexcitation is assumed to follow first order kinetics in the weak absorbance limit of the Beer-Lambert law.
k_{DX}	1.09×10^8 s^{-1}	Decay of the flavin excited singlet state (^{1}F*) by processes other than electron transfer. Value from Supplementary Table C1.
k_{ET}	1×10^{10} s^{-1}	Efficient electron transfer between donor and flavin singlet excited state, ^{1}F*, to form RP1 in the singlet state.
k_{RP2}	2×10^6 s^{-1}	Proton transfer processes to form RP2 from RP1[9].
k_{HFM}	8×10^7 s^{-1}	Coherent singlet-triplet interconversion of the spin states of the geminate radical pair by the hyperfine mechanism. Value from Supplementary Table C1.
k_{RM}	2×10^6 s^{-1}	Incoherent singlet-triplet interconversion of the spin states of the geminate radical pair by the relaxation mechanism. Value from Supplementary Table C1.
$k_{BET(1)}$	2×10^6 s^{-1}	Reverse electron transfer of RP1 to form the ground state species[9].
$k_{BET(2)}$	5×10^4 s^{-1}	Reverse electron transfer of RP2 to form the ground state. Estimated from Ref. [9]

Supplementary Table C2. Values of the rate constants used in calculations of amplified MFEs for the intramolecular flavin photocycle in Supplementary Fig. C5.

Supplementary Fig. C6 shows the *relative* changes in the total concentration of the form of the protein containing the flavin radical [i.e. RP2 plus ($F^{\bullet-}$ D)] while Supplementary Fig. C7 shows the corresponding *absolute* changes. Supplementary Fig. C8 is a repeat of Supplementary Fig. C7 with k_{EX}, the rate constant for photoexcitation, reduced by a factor of 10 to 1×10^2 s^{-1}. Note that Supplementary Fig. C7 is identical to Figs 6d and e in the main text and is reproduced here for comparison with Supplementary Figs. C6 and C8.

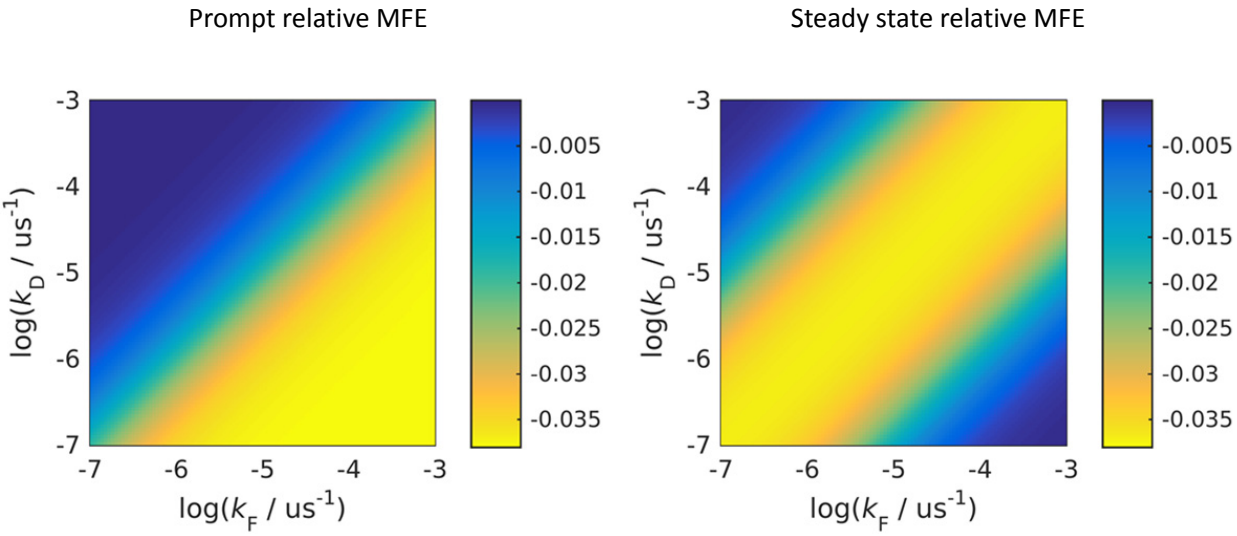

Supplementary Figure C6. Density plot of the relative changes in the total concentration of the flavin radical form of cryptochrome as a function of the radical termination rate constants k_F and k_D. The values of the parameters are given Supplementary Table C2.

The maximum steady state *relative* MFE (Supplementary Fig. C6) is found for $k_F \approx k_D$ and does not exceed the maximum prompt effect (attained for $k_F >> k_D$). While this does demonstrate that slow termination reactions play a role, their impact on the operation of cryptochrome as a magnetic sensor appears to be minor.

The picture is quite different for the corresponding absolute changes (Supplementary Fig. C7). The largest delayed effects occur when $k_D >> k_F$ and they are substantially larger than the prompt effect for any values of k_D and k_F.

Furthermore, when the light intensity is reduced (Supplementary Fig. C8), a larger ratio k_D / k_F is necessary to achieve a significant enhancement (see Supplementary Information). That is, the lower the light intensity the more important is the enhancement phenomenon.

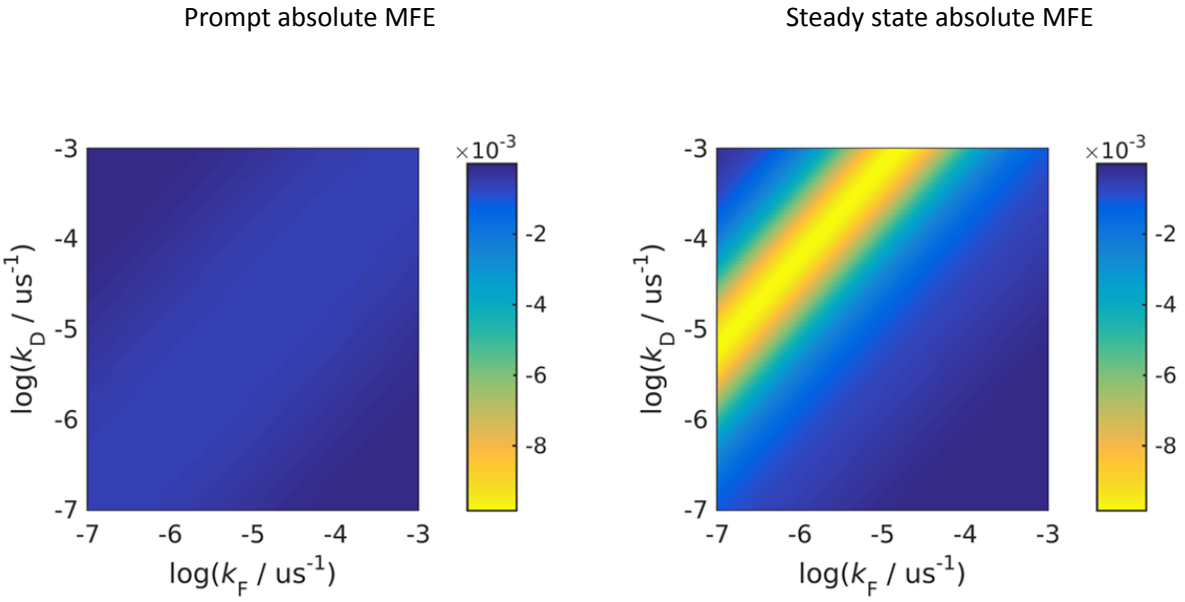

Supplementary Figure C7. Density plot of the absolute changes in the total concentration of the flavin radical form of cryptochrome as a function of the radical termination rate constants k_F and k_D. The values of the parameters are given Supplementary Table C2.

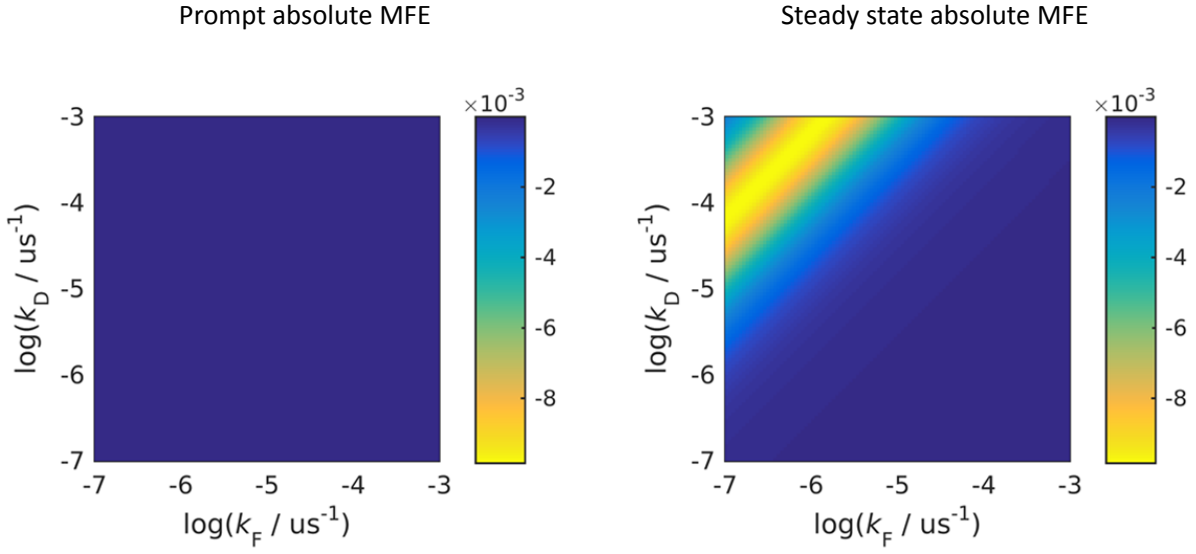

Supplementary Figure C8. Density plot of the relative changes in the total concentration of the flavin radical form of cryptochrome as a function of the radical termination rate constants k_F and k_D. The values of the parameters are given Supplementary Table C2, except that k_{EX} has been reduced by a factor of 10.

D. Bare-bones model of MFEs for inter- and intramolecular radical pairs

The kinetic model described above, while comprehensive, does not readily reveal the essential principles underlying the enhanced MFE. Here we present an approximate, pared down model that shows the same qualitative behaviour and affords a simple expression relating the amplification factor, *E*, to relevant rate constants.

Intermolecular MFEs

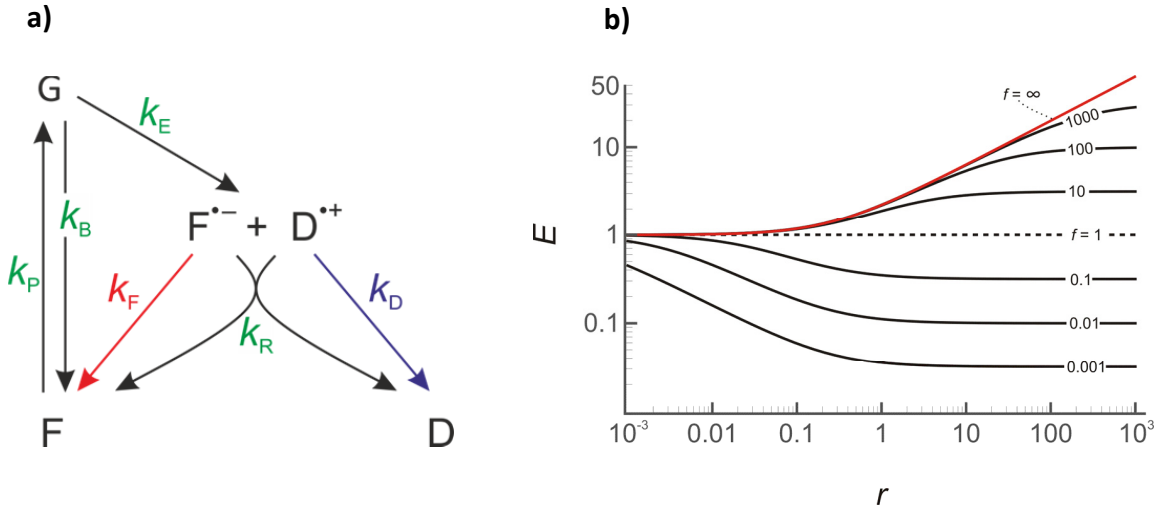

Supplementary Figure D1. a) Simplified reaction scheme for magnetic field effects on intermolecular flavin + donor reactions. The curved arrows indicate a bimolecular process. b) Dependence of the amplification factor *E* on the parameter *r* (defined in the text). The values of $f = k_D/k_F$ are as indicated.

A simplified intermolecular radical pair reaction scheme is shown in Supplementary Fig. D1a. It comprises the diamagnetic, ground-state flavin (F), uncorrelated free radicals ($F^{\bullet-}$ and $D^{\bullet+}$), and a magnetically sensitive intermediate (G), which accounts for the radical pair and all upstream, excited states. Magnetic field effects are introduced by allowing the rate constant with which G returns to F, $k_B(B_0)$, i.e. the recombination efficiency, to depend on the strength of the external magnetic field, B_0. The rate equations are as follows:

$$\begin{aligned}
\frac{d}{dt}[F] &= -k_P[F] + k_B(B_0)[G] + k_F[F^{\bullet-}] + k_R[F^{\bullet-}][D^{\bullet+}] \\
\frac{d}{dt}[G] &= -\left(k_B(B_0) + k_E\right)[G] + k_P[F] \\
\frac{d}{dt}[F^{\bullet-}] &= k_E[G] - k_F[F^{\bullet-}] - k_R[F^{\bullet-}][D^{\bullet+}] \\
\frac{d}{dt}[D^{\bullet+}] &= k_E[G] - k_D[D^{\bullet+}] - k_R[F^{\bullet-}][D^{\bullet+}].
\end{aligned} \tag{4}$$

The prompt MFE (χ_p) is negligibly affected by the slow termination reactions (rate constants k_F and k_D). Thus, to a good approximation, χ_p can be evaluated from the steady state concentrations in the

limit $k_F = k_D = 0$. Using Equation (4) in combination with the requirement that the total concentration of flavin species is fixed,

$$[\mathrm{F}] + [\mathrm{F}^{\bullet-}] = c_0 \tag{5}$$

we find:

$$[\mathrm{F}]_{SS}\left(k_F = k_D = 0\right) = \frac{2c_0k_Rk_B + k_E\left(k_P + 2c_0k_R\right) - \sqrt{k_Ek_P\left(k_Ek_P + 4c_0k_R\left(k_B + k_E\right)\right)}}{2k_R\left(k_B + k_E\right)}. \tag{6}$$

In the general case ($k_F \neq 0$ and $k_D \neq 0$) in which the steady-state concentrations include the additional effects of the termination reactions, we obtain:

$$[\mathrm{F}]_{SS} = \frac{k_Dk_Ek_P + k_F\left(k_B + k_E\right)\left(k_D + 2c_0k_R\right) - \sqrt{k_D\left(k_D\left(k_F\left(k_B + k_E\right) + k_Ek_P\right)^2 + 4c_0k_Rk_Fk_E\left(k_B + k_E\right)k_P\right)}}{2k_F\left(k_B + k_E\right)k_R}. \tag{7}$$

The MFE is defined as the relative change in the steady-state concentration of F brought about by the action of the magnetic field. Since the MFEs, χ_i (i = d, p), are typically small, it is permissible to equate χ_i with a series expansion in k_B truncated after the linear term. Specifically:

$$\chi_i \approx \frac{\mathrm{d}\ln[\mathrm{F}]_{SS}}{\mathrm{d}k_B}\Delta k_B \tag{8}$$

where $[\mathrm{F}]_{SS}$ is given by Equations (6) and (7) for the prompt MFE, χ_p, and the delayed MFE, χ_d, respectively. Δk_B is the field-induced change in k_B. Combining Equations (6), (7) and (8) gives:

$$E = \frac{\chi_e}{\chi_p} = \frac{k_D\sqrt{k_Ek_P\left(k_Ek_P + 4c_0k_R\left(k_B + k_E\right)\right)}}{\sqrt{k_D\left(k_D\left(k_F\left(k_B + k_E\right) + k_Ek_P\right)^2 + 4c_0k_Rk_Fk_Ek_P\left(k_B + k_E\right)\right)}}. \tag{9}$$

Since k_D and k_F are assumed small compared to the other rate constants, Equation (9) can be expanded in powers of these rate constants, keeping their ratio constant, $f = k_D/k_F$, constant. Retaining only the first term, we obtain:

$$E = \sqrt{\frac{1+4r}{1+4r/f}} \tag{10}$$

where $r = \left(k_Rc_0\right)/\left(\phi_Ek_P\right)$ and $\phi_E = k_E/\left(k_E + k_B\right)$ denotes the quantum yield for the formation of free radicals. When r >> 1 and r >> f, Equation (10) implies that $E \approx \sqrt{f}$. Supplementary Fig. D1b illustrates the dependence of E on r for different ratios of k_D and k_F. When r is greater than about 100, E is indeed seen to be proportional to $\sqrt{f}$.

Intramolecular MFEs

Amplified MFEs can also occur for radical pairs formed intramolecularly in a photocycle in which there are no bimolecular recombination reactions. A bare-bones reaction scheme that qualitatively accounts for MFEs in this case is shown in Supplementary Fig. D2a. Proceeding in a manner analogous to that for the intermolecular case, we find that the MFE enhancement for the ground-state (F–D) is given by

$$E = \frac{f^2 + f + 1}{\kappa f^2 + f + \kappa} \tag{11}$$

where $\kappa = k_P / [k_P + k_B(B_0)]$. Note that when $k_F = k_D = 0$, the MFE is $\chi_p = \kappa \Delta k_B / k_B$. For an experiment that detects the fluorescence of the electron acceptor, F (see Supplementary Fig. D2a), Equation (11) is applicable when the photoexcited state of F is swiftly quenched in the state $F–D^{\bullet+}$, e.g. by energy transfer. Note that $\kappa \leq 1$ so that an enhancement of the MFE ($E \geq 1$) is expected irrespective of the value of $f = k_D/k_A$. This is strikingly different to the intermolecular case above.

If the populations of both $F–D^{\bullet+}$ and F–D are monitored via the fluorescence of F, the enhancement factor is given by:

$$E = \frac{f^2 + f + 1}{\kappa f^2 + f + \kappa} - \frac{1}{f(1-\kappa) + \kappa} \tag{12}$$

and significant MFE enhancement results for $f > 1$. If the fluorescence quantum yield is reduced by the presence of $D^{\bullet+}$, Eqs. (12) and (11) provide lower and upper bounds on E. Supplementary Fig. D2b illustrates the dependence of E on f in these two limits.

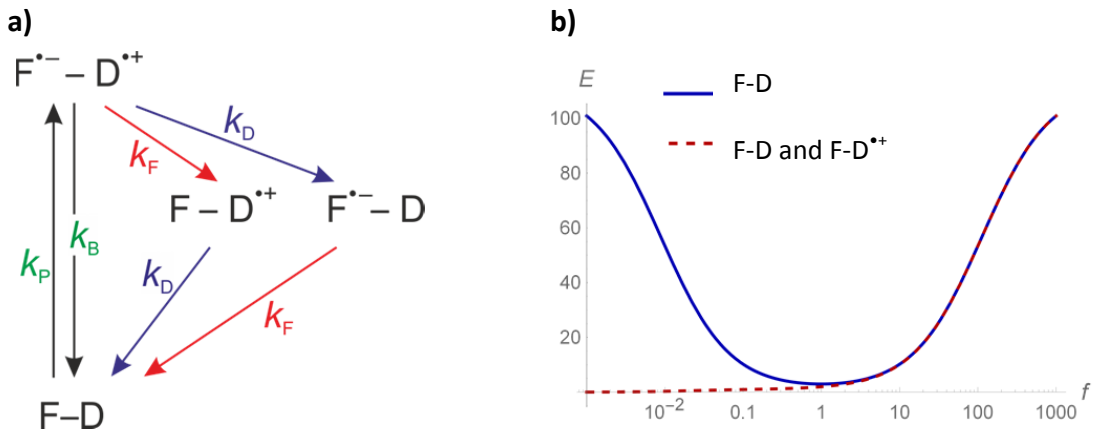

Supplementary Figure D2. **a**, Simplified reaction scheme for magnetic field effects on intramolecular flavin + donor reactions. **b**, Dependence of the enhancement factor E on $f = k_D/k_F$ for $\chi_p = 0.89\%$. The blue line gives the MFE on the ground-state population. The dashed red line gives the MFE on the total concentration of F irrespective of the oxidation state of the donor. The two calculations predict almost identical E when $f > 2$.

E. Flavin photochemistry

Transient absorption

Transient absorption spectra for the FMN/lysozyme and FMN/Trp reactions were obtained using a Sirah Cobra Dye laser (450 nm, 3 mJ, 7 ns pulses) pumped by a Nd:YAG Continuum Surelite laser (355 nm, 100 mJ, 7 ns pulses). An Oriel xenon arc lamp (800 W) provided the continuous UV-visible probe light. The probe light transmitted through the sample cell was passed to an Oriel monochromator to select a specific wavelength and then detected by a photo-multiplier tube. The time-resolved absorption profile, $\Delta A(t)$, was recorded as the difference in the absorption of the sample before and after photoexcitation, as a function of time after the pump pulse.

The transient absorption spectra for FMN/lysozyme and FMN/Trp (Supplementary Fig. E1) show that the flavin triplet excited state, ^{3}FMN*, and the neutral flavin semiquinone radical, FMNH$^\bullet$, decay on the order of microseconds and seconds respectively, in agreement with prior studies.[10, 11] A Stern-Volmer plot for ^{3}FMN* gave a ^{3}FMN*–Trp quenching rate constant of 1.2×10^9 $M^{-1}s^{-1}$ close to the diffusion controlled limit.

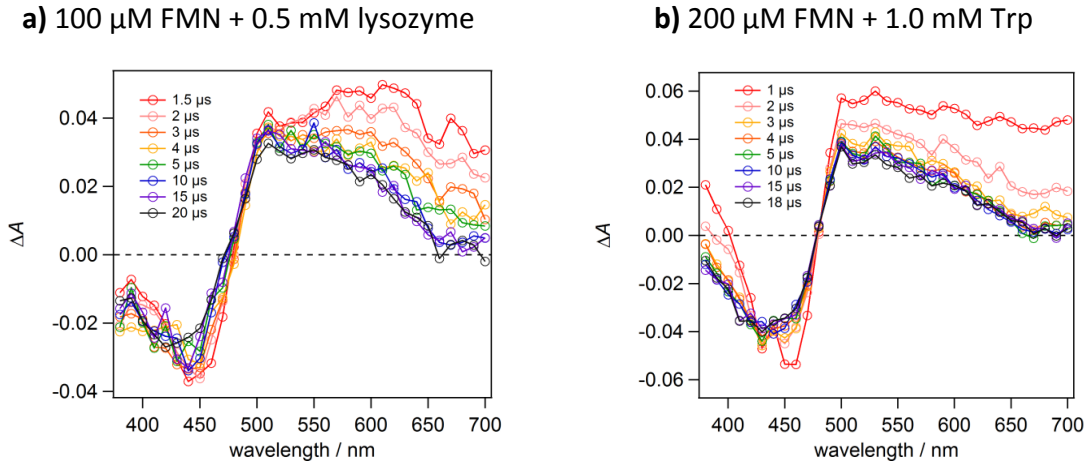

Supplementary Figure E1. Transient absorption spectra for a) FMN/lysozyme (triplet lifetime = 2.15 ± 0.01 µs) and b) FMN/tryptophan (triplet lifetime = 0.62 ± 0.01 µs) in aqueous solution.

Reactivity of flavin radicals

A significant reaction pathway for the neutral flavin semiquinone radical is the thermodynamically favourable disproportionation reaction to form the fully oxidized and fully reduced forms of the flavin:

$$2\mathrm{FH}^\bullet \rightarrow \mathrm{FH_2} + \mathrm{F}. \qquad (13)$$

The disproportionation and comproportionation reactions having rate constants: $k_{dis} = 5 \times 10^8$ $M^{-1}s^{-1}$ and $k_{com} = 1 \times 10^6$ $M^{-1}s^{-1}$, respectively.[12, 13] Oxidation of the fully reduced flavin by activated oxygen species such as hydrogen peroxide can recover the oxidized flavin:

$$\mathrm{FH_2} + \mathrm{H_2O_2} \rightarrow \mathrm{F} + 2\mathrm{H_2O}\ . \qquad (14)$$

Furthermore, there is a slow reaction pathway for the neutral semiquinone radical reacting with molecular oxygen[12, 13] with a rate constant $k_{O_2} \approx 1 \times 10^4$ $M^{-1} s^{-1}$:

$$FH^{\bullet} + O_2 \rightarrow F + O_2^{\bullet -} + H^+ . \quad (15)$$

However, oxidation of $FH^{\bullet}$ radicals by the superoxide ($O_2^{\bullet -}$) formed in (15),

$$FH^{\bullet} + O_2^{\bullet -} + H^+ \rightarrow F + H_2O_2 , \quad (16)$$

occurs much more rapidly ($k_{O_2^{\bullet -}} \approx 1 \times 10^8$ $M^{-1} s^{-1}$), meaning that the two reactions together are autocatalytic.[13]

The disproportionation and molecular oxygen reactions are obvious candidates for MFE-enhancing termination processes in intermolecular photocycles. Both reactions proceed with a supra-linear dependence on the concentration of flavin radicals resulting in a reduction in k_D/k_F, and hence also in E, when either the flavin concentration or the pump power is increased (see above and main text).

Furthermore, the rate of reaction of flavin radicals with molecular oxygen is strongly dependent on their protonation state (pK_a(FMNH$^{\bullet}$) = 8.6) and therefore on the pH. The equivalent reaction to (15) for FMN$^{\bullet -}$ has a rate constant, $k_{O_2} \approx 1 \times 10^8$ $M^{-1} s^{-1}$, that is four orders of magnitude faster than for FMNH$^{\bullet}$.[12, 13] This allows E to be controlled by changing the pH of the solution.

To confirm the involvement of molecular oxygen, experiments were performed on de-oxygenated aqueous solutions of FMN (10 μM) and tryptophan (1.0 mM) prepared in a glove box under an argon atmosphere (Supplementary Fig. E2). Consistent with the above interpretation, we found an increased amplification factor (E) in the absence of oxygen because of the reduced rate of removal of flavin radicals (k_F). The absolute amplitude of the prompt magnetic field effect is also slightly higher, probably due to a longer radical pair lifetime. De-oxygenation has an impact at several points in the photocycle (unlike, for example, adding TCEP whose only significant effect is to accelerate the reduction of the donor radical). In the absence of oxygen, flavin triplets accumulate leading to triplet-triplet annihilation ($T_1 + T_1 \rightarrow S_1 + S_0$) and delayed fluorescence ($S_1 \rightarrow S_0 + h\nu_F$) which complicates matters considerably. Additionally, in the absence of oxygen, the flavin radicals are very long lived meaning that there is a much greater depletion of the ground state reactants and consequently weak fluorescence from the desired route ($S_0 + h\nu \rightarrow S_1$; $S_1 \rightarrow S_0 + h\nu_F$). In short, the presence of oxygen is desirable in the sense that it “closes” the photocycle and gives favourable cycle times.

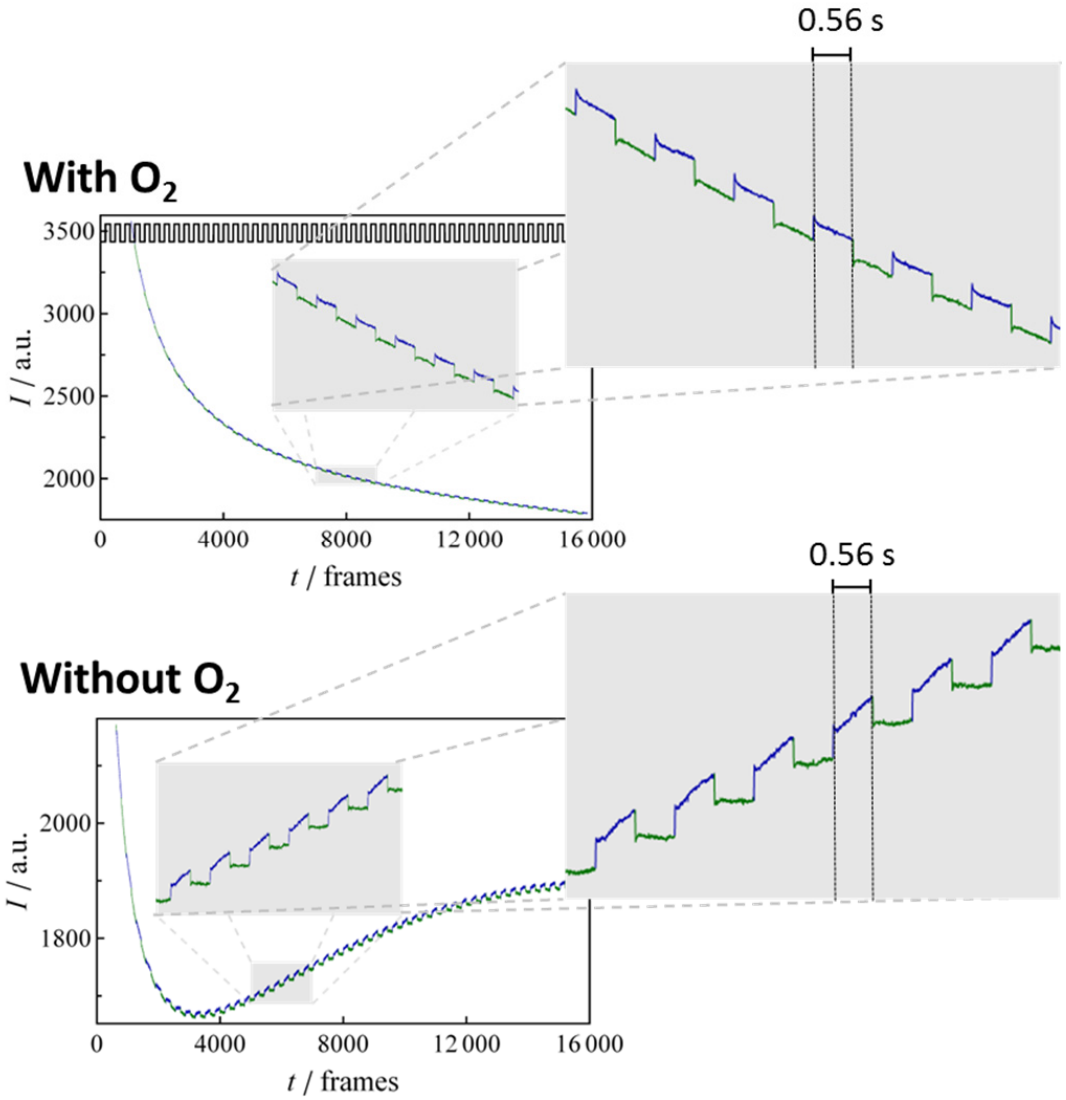

Supplementary Figure E2. Fluorescence intensities of aqueous solutions of FMN (10 μM) and tryptophan (1.0 mM) recorded under oxygenated and de-oxygenated conditions.

F. Switched light intensity

Corroboration of our interpretation of the MFE amplification effect was obtained from experiments in which the light intensity was periodically adjusted (in the absence of a magnetic field) as an alternative way of shifting the position of the photo-stationary state (Supplementary Fig. F1a). Attenuation of the light intensity was achieved by square-wave, on-off modulation of the 350 mW laser output varying the duty cycle to obtain the reduced intensities (80%, 70%, 60%, 50% and 20%) shown in the figure. When the light intensity was abruptly reduced, a prompt fluorescence component was observed followed by a slow delayed component. This is reproduced by simulations (Supplementary Fig. F1b) with the same parameter values used previously (Supplementary Table C1).

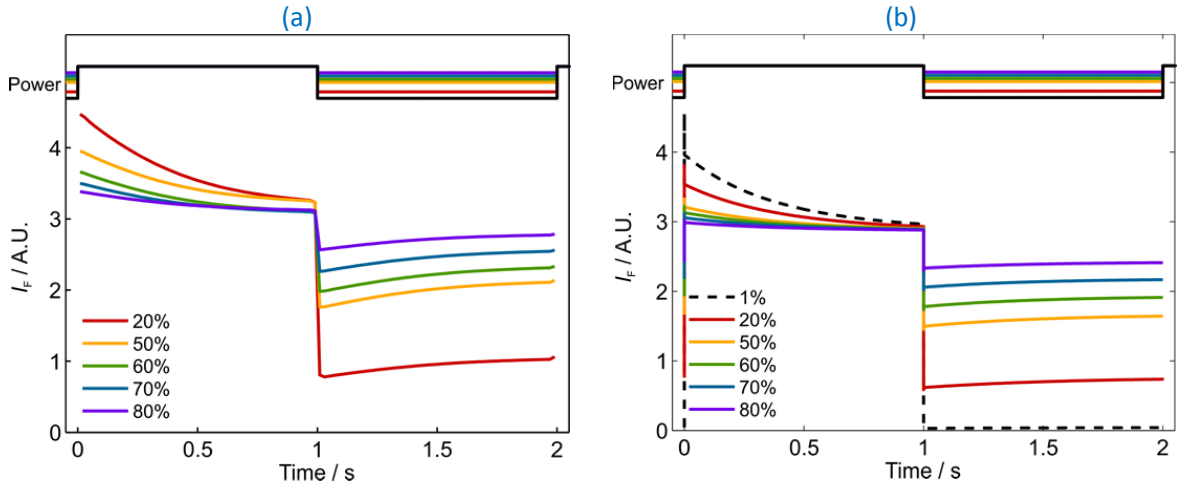

Supplementary Figure F1. (a) Fluorescence intensities of an aqueous solution of FMN (10 μM) and lysozyme (0.5 mM) recorded using a 405 nm diode laser. The laser power (350 mW) was periodically attenuated by 20–80% after 1.0 s of irradiation and returned to 350 mW after a further 1.0 s. (b) Simulation of this experiment using $k_F = 1\ s^{-1}$, $k_D = 10.0\ s^{-1}$, $k_{EX} = 1.73 \times 10^3\ s^{-1}$ and other parameter values as in Supplementary Table C1.

Supplementary References

1. Evans E. W., *et al.* Sensitive fluorescence-based detection of magnetic field effects in photoreactions of flavins. *Phys. Chem. Chem. Phys.* **17**, 18456-18463 (2015).
2. Courson D. S. & Rock R. S. Fast benchtop fabrication of laminar flow chambers for advanced microscopy techniques. *Plos One* **4**, e6479 (2009).
3. Dodson C. A., *et al.* Fluorescence-detected magnetic field effects on radical pair reactions from femtolitre volumes. *Chem. Commun.* **51**, 8023-8026 (2015).
4. Press W. H., Teukolsky S. A., Vetterling W. T. & Flannery B. P. *Numerical Recipes 3rd edition: The Art of Scientific Computing*. Cambridge University Press: Cambridge, 2007.
5. Holzer W., *et al.* Photo-induced degradation of some flavins in aqueous solution. *Chem. Phys.* **308**, 69-78 (2005).
6. Murakami M., Maeda K. & Arai T. Dynamics of intramolecular electron transfer reaction of FAD studied by magnetic field effects on transient absorption spectra. *J. Phys. Chem. A* **109**, 5793-5800 (2005).
7. Losi A., Polverini E., Quest B. & Gartner W. First evidence for phototropin-related blue-light receptors in prokaryotes. *Biophys. J.* **82**, 2627-2634 (2002).
8. Holzer W., Penzkofer A., Fuhrmann M. & Hegemann P. Spectroscopic characterization of flavin mononucleotide bound to the LOV1 domain of Phot1 from *Chlamydomonas reinhardtii*. *Photochem. Photobiol.* **75**, 479-487 (2002).
9. Maeda K., *et al.* Magnetically sensitive light-induced reactions in cryptochrome are consistent with its proposed role as a magnetoreceptor. *Proc. Natl. Acad. Sci. USA* **109**, 4774-4779 (2012).
10. Miura T., Maeda K. & Arai T. Effect of coulomb interaction on the dynamics of the radical pair in the system of flavin mononucleotide and hen egg-white lysozyme (HEWL) studied by a magnetic field effect. *J. Phys. Chem. B* **107**, 6474-6478 (2003).
11. Tsentalovich Y. P., Lopez J. J., Hore P. J. & Sagdeev R. Z. Mechanisms of reactions of flavin mononucleotide triplet with aromatic amino acids. *Spectrochim Acta A* **58**, 2043-2050 (2002).
12. Massey V. Activation of molecular-oxygen by flavins and flavoproteins. *J. Biol. Chem.* **269**, 22459-22462 (1994).
13. Vaish S. P. & Tollin G. Flash photolysis of flavins. V. Oxidation and disproportionation of flavin radicals. *J. Bioenerg.* **2**, 61-72 (1971).